Combination of ERDA, FTIR spectroscopy and NanoSIMS for the characterization of hydrogen incorporation in natural diamonds

Divine Vangu, Hélène Bureau, Hicham Khodja, Matthieu Charrondiere, Imène Esteve, Keevin Béneut, Laurent Remusat, Eloïse Gaillou, Pierre Cartigny, Jean-Claude Bouillard

Combination of ERDA, FTIR spectroscopy and NanoSIMS for the characterization of hydrogen incorporation in natural diamonds

Divine Vangu[a]*, Hélène Bureau[a], Hicham Khodja[b], Matthieu Charrondiere[a], Imène Esteve[a], Keevin Béneut[a], Laurent Remusat[a], Eloïse Gaillou[c], Pierre Cartigny[d], Jean-Claude Bouillard[a]

[a]Institut de Minéralogie, de Physique des Matériaux et de Cosmochimie (IMPMC), Sorbonne Université, MNHN, CNRS UMR 7590, 75252 Paris Cedex 5, France

[b]Université Paris-Saclay, CEA, CNRS, NIMBE, LEEL, 91191, Gif-sur-Yvette, France

[c]Mines Paris – PSL, PSL University, Musée de Minéralogie, 60 boulevard Saint-Michel, 75006 Paris, France

[d]Institut de Physique du Globe de Paris, Université de Paris, 75005 Paris, France

Corresponding author: divine.vangu_mpaka@sorbonne-universite.fr

Keywords: ERDA, FTIR, NanoSIMS, Natural diamonds, Hydrogen

Highlights.

- Hydrogen is the second major impurity in natural diamonds
- ERDA measurements show that natural diamonds contain up to 25 wt. ppm of hydrogen
- Hydrogen content in natural diamonds is not correlated with nitrogen content
- Hydrogen content in natural diamonds depends on growth habit
- No chemical equilibration of diamonds' hydrogen by diffusion through geological times

Abstract.

Hydrogen is a volatile element involved in several geological processes ranging from rock weakening to the initiation of tectonic plates. Because it is present in diamond, the investigation of hydrogen content in natural diamonds could provide valuable information. Such studies are scarce despite hydrogen being among the main impurities in their structure. Using Elastic Recoil Detection Analysis, Fourier Transform Infrared spectroscopy and Nanoscale Secondary Ions Mass Spectrometry, we analyzed the incorporation of hydrogen in three diamonds growth habits: octahedral, cuboid and fibrous. Up to 25 wt. ppm of hydrogen was measured in some samples, placing hydrogen as the second most abundant impurity in natural diamonds after nitrogen and before boron. Comparison between the three methods indicates a difference in the main mode of hydrogen incorporation depending on the growth habit. Hydrogen is more readily incorporated in the fibrous and cuboid habits compared to the octahedral one. We also show that the incorporation of hydrogen is not correlated with the incorporation of nitrogen. Results suggest no chemical equilibration of hydrogen by diffusion through geological times and also confirm that not all hydrogen may be infrared active.

1. Introduction.

Natural diamonds are the deepest geological samples which formation occurs at depth from 150 to more than 800 km [1]. They contain a large wealth of information about the Earth mantle, either through their crystalline structure [2] or the fluid and mineral inclusions encapsulated inside [1], making them unique witnesses of the deep Earth interior and of its history. Hydrogen (H) is among the most abundant impurities in natural diamonds along with nitrogen [3,4] and boron [5]. The presence of H plays an important role in several geological processes that take place in its interior: from weakening the structure of rocks and minerals [6,7] to the possible initiation of tectonic plates [8–10]. Studies on the incorporation of H in

minerals have proposed the existence of a cycle within the Earth interior and that a significant amount of H is stored in the deep Earth [11,12]. Characterizing the incorporation of H in natural diamonds and their inclusions constitutes an indirect way to study its cycle in the deep Earth (from the lithosphere to the core-mantle boundary) and thus helps at understanding the geological processes that led to the evolution of our planet. How H is incorporated and distributed in natural or synthetic diamonds is also crucial in gemology since it changes the color of the gem[13] but also in material sciences since H is a poison in high-tech diamonds applications [14].

Aside from a few pioneer studies [15–19], the total H content of natural diamonds has not been studied much. The quantity of incorporated H, although suggested to go from a few up to 4000 at. ppm (338 wt. ppm) [18,20], is still not precisely known. For the past two decades or so, H content in natural diamonds has mainly been studied using Fourier Transform Infrared (FTIR) spectroscopy. The presence of H leads to a series of infrared active defects as indicated by the numerous absorption bands [21,22]. The height (or area) of the band at 3107 cm^{-1}, considered as the major absorption band and related to a C–H bond in the N_3VH defect [23,24], is used to estimate if a diamond is “H rich” [25]. Real quantification, however, is not possible due to the lack of knowledge of the absorption coefficient of each H related absorption band. FTIR is also limited because of its dependence on the structure of the H related defects. It was also conjectured that not all H is infrared active [18], making any quantification using FTIR highly questionable.

Elastic Recoil Detection Analysis (ERDA), an ion beam analysis technique already applied to a wide range of materials, can be used to quantify the H content in natural diamonds. Contrarily to FTIR, ERDA is a speciation and calibration independent technique, allowing the absolute quantification of H [26]. The technique has been greatly improved in term for spatial resolution [26,27], allowing its application on geological samples such as nominally anhydrous minerals (NAMs) [28,29], silicates glasses [30,31] and metallic phases [30,32]. ERDA is also routinely employed to calculate the absorption coefficient of water related infrared absorption bands in NAMs [31,33] or to obtain the standards needed for the quantification in Secondary Ions Mass Spectrometry (SIMS) [34–36]. We present here the combined use of ERDA, FTIR and NanoSIMS for the characterization of H in natural monocrystalline diamonds of octahedral, fibrous and cuboid growths. The absolute H content was measured in various areas of the samples using ERDA and compared to H-related absorption bands to evaluate its infrared active proportion. NanoSIMS was used to check the homogeneity of H distribution at the microscale. Finally, we compared results of each method to determine if the amount of H and its mode of incorporation changes among the three growth habits.

2. Materials and Methods.

2.1. Analyzed samples.

For this study, we choose samples among the most common types of diamonds found in nature [37].

These four natural type Ia diamonds exhibit three different growths: octahedral, fibrous and cuboid (Figure S1). They are (1) two monocrystalline octahedral diamonds (PCS6, VEN03), which are typical of natural diamonds from lithospheric cratons (2) one coated diamond (CARTI1), having an octahedral core surrounded by a fibrous diamond rim, fibrous diamonds consisting of microscopic parallel fibers; (3) and one asteriated diamond (ASTER) presenting the association of octahedral sectors together with cuboid sectors which are well known to contain detectable and possibly significant amounts of hydrogen [38].

PSC6 is a commercial diamond window from Almax EasyLab, while ASTER is a mirror polished asteriated diamond from Marange alluvial deposits in Zimbabwe. Asteriated diamonds are characterized by the simultaneous growth of the octahedral and cuboid sectors [38], which appear transparent and grey respectively (Figure S1). CARTI1 is a coated diamond from Democratic Republic of Congo. VEN03 is a monocrystalline octahedral rough diamond from the alluvial deposit in Santa Elena de Uairén in Venezuela which we polished using an Ion Beam Milling System at -120°C following the protocol described previously [39] to expose one of its olivine inclusions. All samples were carbon coated for the ERDA and CARTI1 was also gold coated for the NanoSIMS analysis.

2.2. Elastic Recoil Detection Analysis.

The total H contents of each diamond were determined by ERDA using the nuclear microprobe at the Laboratoire d'Etude des Elements Légers (LEEL) in CEA Saclay, France [40]. A detailed description of the followed analytical procedure can be found in the literature [26,27]. In brief, a 2.8 MeV, 500 pA $^{4}He^{+}$ ion beam was focused to 2×2 μm^2 and raster scanned to 200×200 μm^2 on samples' surface. An 11 μm thick aluminum foil is placed in front of the ERDA detector to stop the transmission of forward scattered $^{4}He^{+}$ particles. The resulting investigated depth is of 215 nm. The experimental setup permits to conduct simultaneously Rutherford Backscattering (RBS), used to monitor the elemental composition and the total deposited charge. Solid angles for both RBS and ERDA detectors were measured using a set of standards (Al_2O_3, $CaCO_3$, FeS_2, SiO_2 and Zr for RBS; Kapton ($C_{22}H_{10}O_5N_2$), plus two glass standards: 2πD45 [41] and STR10 [26] for ERDA). ERDA and RBS spectra were acquired during 3600 or 7200 s and measurements were conducted on various areas of each sample. We evaluated the detection limit using the residual ERDA signal from a nominally anhydrous San Carlos olivine (0.16 wt. ppm H [42], Figures S2). Transposed to a diamond matrix, this detection limit is 6 wt. ppm. H content. Uncertainties take into account the Poisson statistical counting contribution and those originating from spectrum energy calibration, measured RBS and ERDA solid angles and tilt angle of the sample holder [27]. RBS and ERDA spectra were processed using the modeling software SIMNRA [43].

2.3. Fourier Transform Infrared spectroscopy.

Infrared analyses were made using a Nicolet 6700 (Thermofisher) IR spectrometer equipped with an IR-Plan microscope at the spectroscopic platform of the Institut de Minéralogie, de Physique des Matériaux et de Cosmochimie (IMPMC) at Sorbonne Université, France. A spectrum was recorded at each ERDA mark between 400 and 7000 cm^{-1} in transmission mode with an aperture of 100x100 μm^2. 128 scans were collected for each spectrum with a spectral resolution of 4 cm^{-1}. We used the DiaMap and DiaMapFluid Excel spreadsheets [44] to calculate the height of selected H related absorption bands and determine the total nitrogen content of each sample.

2.4. Nanoscale Secondary Ions Mass Spectrometry.

H contents were determined by NanoSIMS. Measurements were conducted on the Cameca NanoSIMS 50 installed at Muséum National d'Histoire Naturelle (MNHN) in Paris, France to check the homogeneity of H distribution at the microscale. Secondary ions of $^{12}C^{-}$, $H^{12}C^{-}$, $^{12}C^{12}C^{-}$ and $^{13}C^{12}C^{-}$ were collected by electron multipliers in multicollection mode to obtain H contents. The calibration needed for quantification was made of a set of diamond standards whose H content was determined by ERDA: a type Ia natural diamond (15 wt. ppm) and a synthetic type IIa diamond (13 wt. ppm) [45], and an implanted type Ia natural diamond (70 wt. ppm). The primary Cs^{+} beam was set to 1 pA and was scanned over a surface area of 5×5 μm^2. To avoid surface contamination, only ions from the inner 2×2 μm^2 region were

collected with the “beam blanking mode”. Each analysis consisted in a stack of 100 cycles, with each stack lasting 4.096 s. Mass resolving power was set at minimum 9000, enough to resolve interferences on measured secondary ions. Before each analysis, a 7×7 µm^2 surface area was initially pre-sputtered for 300 s with a 250 pA primary Cs^+ rastering beam, in order to remove the gold coating and reach a sputtering steady-state [46]. AFM measurements show that the depth investigated is of about 120 nm. An electron flooding gun was used for charge compensation at the surface of the sample to improve the secondary ions emission.

3. Results.

3.1. ERDA and NanoSIMS results.

ERDA results are exemplified in Figure 1, which displays the RBS (1A, 1C) and ERDA (1B, 1D) spectra of one analyzed region of ASTER and the olivine inclusion of VEN03. Two contributions can be seen on the ERDA spectra (Figures 1B, 1D): (1) the large peak at high energy due to the H surface contamination; (2) the counts at lower energies coming from the H situated deeper in the sample. The grey region on the ERDA spectra indicates the region of interest used to evaluate the H content in each analyzed region.

Table 1. Results of ERDA, NanoSIMS and FTIR analyses.

Sample	Probed region	H content (ERDA, wt. ppm)	H content (NanoSIMS, wt. ppm)	H peaks height (FTIR, cm^{-1})	Fluid inclusions H content (FTIR, wt. ppm)	N content (FTIR, wt. ppm)
PSC6	Octahedral	5 – 9	-	0.01 – 0.07	-	1370 – 1470
VEN03	Octahedral	5 – 9	-	0.10 – 0.20	-	1020 – 1120
	Olivine incl.	8	-	-	-	-
ASTER	Cuboid	16 – 21	-	40.0 – 50.0	-	1990 – 2320
	Octahedral	5 – 12	-	4.0 – 8.0	-	3080 – 3280
CARTI1	Fibrous	12 – 23	10 – 14	1.5 – 2.0	5 – 15	1250 – 1390
	Octahedral	5 – 9	8 – 11	0.10 – 1.5	-	1120 – 1440

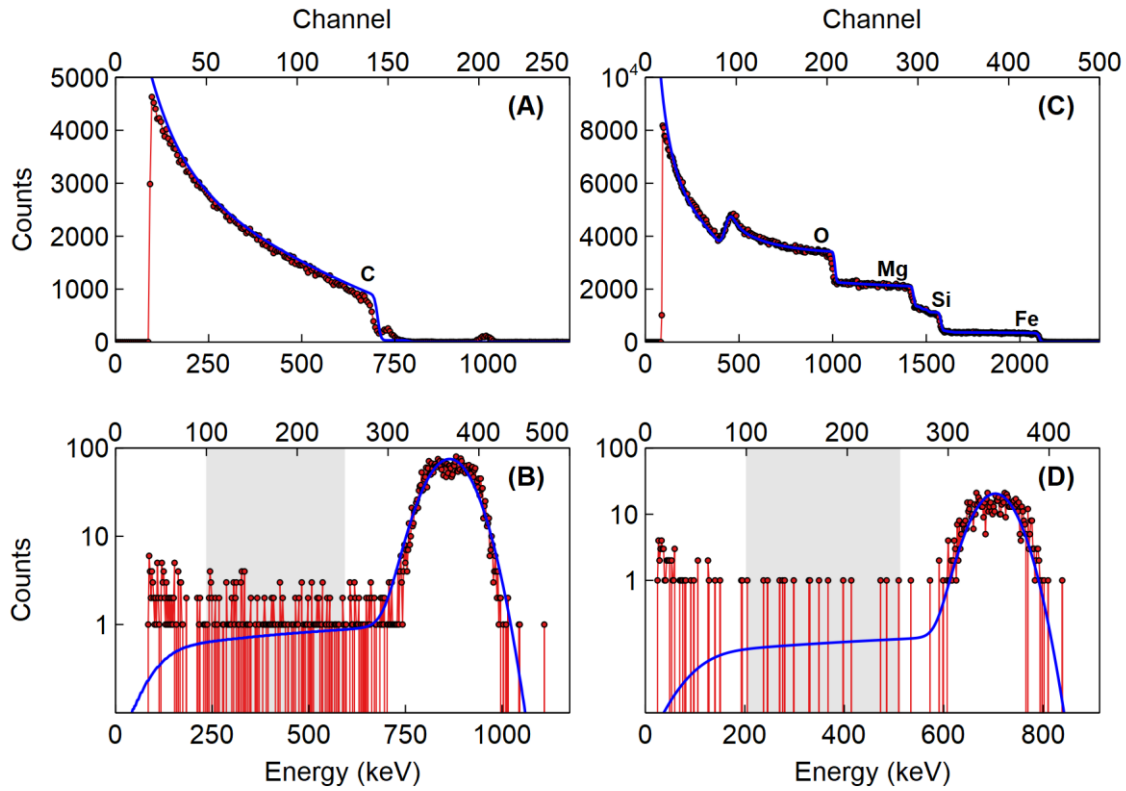

Figure 1. (A) RBS and (B) ERDA spectra of the cuboid sector of ASTER. (C) RBS and (D) ERDA spectra of the olivine inclusion of VEN03. The counts are given in logarithmic scale. The simulated spectra (blue) represent the fit of the experimental spectra (red).

With ERDA, the highest H contents were measured in the cuboid growth of ASTER and the fibrous growth of CARTI1 with values ranging from 12 to 23 wt. ppm (Table 1). The H contents of the octahedral growth of each diamond was significantly lower: CARTI1, PSC6 and VEN03 contained between 5 to 9 wt. ppm of total H while the values for ASTER were slightly higher, going up to 12 wt. ppm (Table 1). We also determined the H content of the olivine inclusion of VEN03 (Figure 1), which contained 8 wt. ppm. The H contents measured by NanoSIMS for CARTI1 ranged from 8 to 11 wt. ppm for the octahedral habits and from 11 to 14 wt. ppm for the fibrous habit (Table 1). The relative error was of 10–20% for ERDA and of 3–5% for NanoSIMS (Tables S2 and S8).

3.2. FTIR results.

We identified four kinds of FTIR spectra: two for the octahedral growth habits, one for the cuboid sector of ASTER and another for the fibrous sector of CARTI1 (Figure 2). In the case of the octahedral growth, the absorption of the hydrogen related features was so weak that either none could be detected or only the line at 3107 cm-1 could be seen. Contrarily, the FTIR spectrum of the cuboid sector of ASTER is characterized by several absorption bands related to the presence of H. Among them are the bands related to the N_3VH defect [24] at 1405, 2786 and 3107 cm^{-1}. Other bands identified in the literature [21,22] are also present at 3050, 3124, 3145, 3155, 3236, 3190 and 3310 cm^{-1}. Lastly, the FTIR spectrum of the fibrous sector of CARTI1 is characterized by the presence of three thin and relatively low in intensity bands at 3107, 3236 and 3310 cm^{-1} but also by two much broader bands at 1642 and 3421 cm^{-1} (Figure 2C, Figure S10). The last two bands are respectively associated to the H–O–H bending and the O–H stretching which indicates the presence of water in the fibrous sector of CARTI1 [47]. We calculated up to 15 wt. ppm of hydrogen in the water detected in the fibrous sector of

CARTI1 using the absorption coefficient leading to the highest value in DiaMapFluid (87 AU.L.mol^{-1}.cm^{-1}) [48].

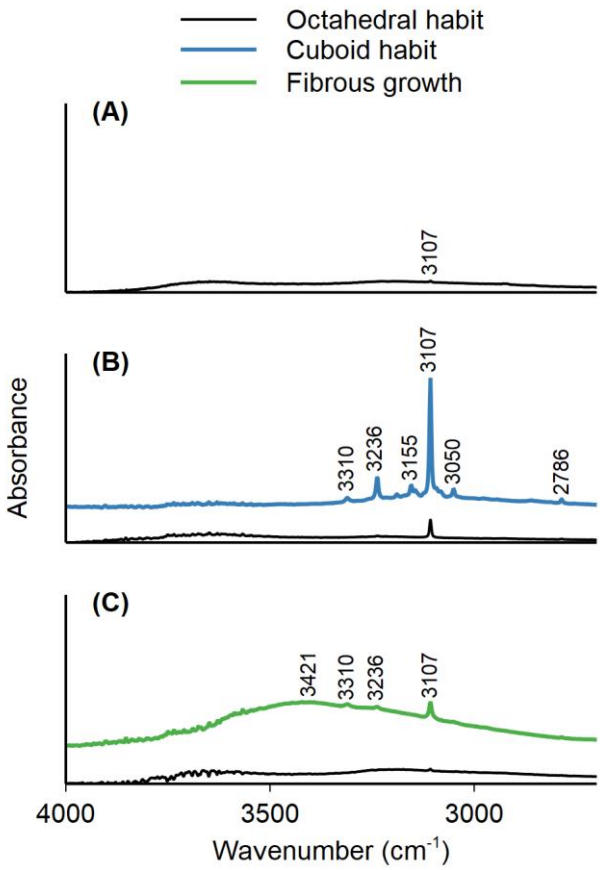

Figure 2. FTIR spectra of the H-related absorption region for the different growths of (A) VEN03, (B) ASTER and (C) CARTI1. Black line: Octahedral habit. Blue line: Cuboid habit. Green line: fibrous habit. The full FTIR spectra can be found in the supporting information (Figure S10).

The highest values were measured in ASTER with values ranging from 40 to 50 cm^{-1} for the cuboid growth and values ranging from 4 to 8 cm^{-1} for the octahedral one (Table 1). The lowest values came from the octahedral habits of CARTI1, PSC6 and VEN03 and ranged from nearly zero to 1.5 cm^{-1} (Table 1).

Each octahedral growth had a different N content. The highest values were measured in the octahedral and cuboid sectors of ASTER with values ranging from 3080 to 3280 wt. ppm and 1990 to 2320 wt. ppm, respectively. We measured between 1020 and 1120 wt. ppm for VEN03, between 1370 and 1470 wt. ppm for PSC6. Finally, we measured between 1120 and 1440 wt. ppm of nitrogen for the octahedral core of CARTI1 and between 1250 and 1390 wt. ppm for its fibrous coat.

3.3. Comparison between ERDA and FTIR results.

Despite the lack of any H-related IR absorption band for PSC6 (Figure S10A), its H content (from ERDA) is almost identical to the values for the octahedral sector of CARTI1 and VEN03 which both display the 3107 cm^{-1} absorption band. The octahedral sector of ASTER shows a much higher absorption band at 3107 cm^{-1} than the other octahedral growths and is also associated to a higher H content. Both the cuboid growth of ASTER and the fibrous growth of

CARTI1 show the highest H content of all growths but the H peaks height of ASTER is almost twenty times higher than in CARTI1.

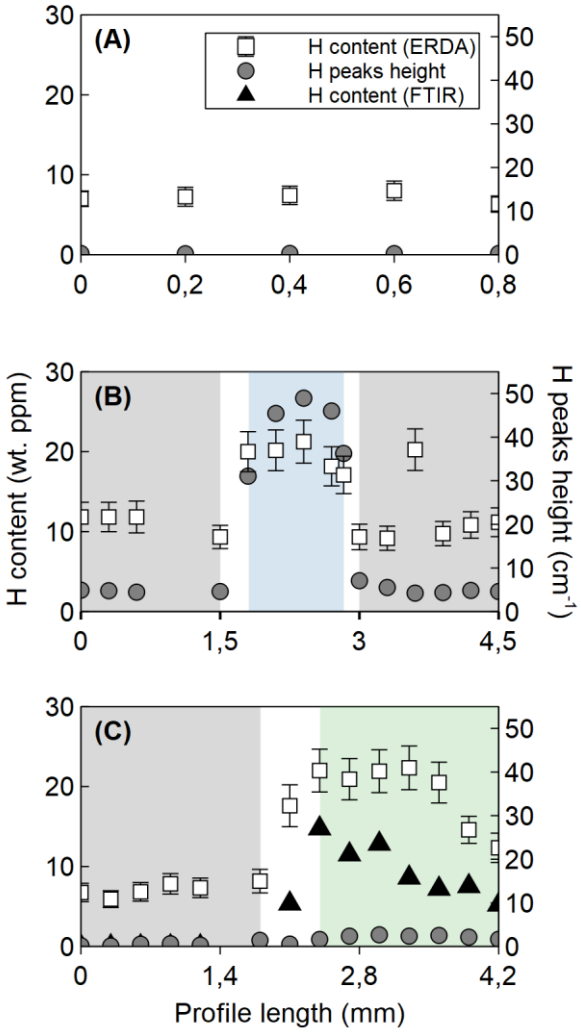

Figure 3. Profile of the total H content (ERDA, white squares), H peaks height (FTIR, grey circles) and H content of water (FTIR, black triangles) in (A) VEN03, (B) ASTER and (C) CARTI1. Grey region: Octahedral habit. Blue region: Cuboid growth (ASTER). Green region: Fibrous growth (CARTI1). The high H content value in the octahedral sector of ASTER is due to the presence of a fracture on the analyzed area. Additional profiles made in ASTER can be found in the supporting information (Figure S11).

For ASTER, the H content and the H FTIR peaks height of its octahedral sector are much higher than in the octahedral growth of any other diamond. When passing to the cuboid sector, these values increase with the H content almost doubling (from 10 to 20 wt. ppm, Figure 3) while the H peaks height is multiplied by ten (from 5 to 50 cm^{-1}, Figure 3B).

In the case of CARTI1, the FTIR profile of the octahedral sector is similar to VEN03's with a low (if not almost absent) H peaks height associated to a H content of 5–8 wt. ppm (Figure 3A, 3C). Within the fibrous sector, the ERDA and FTIR results branch out. The H content reaches values up to 23 wt. ppm while the H peaks height goes up to 2 cm^{-1}, which remains lower than the octahedral sector of ASTER. Because of the presence of water on the FTIR spectrum of the fibrous growth of CARTI1, we also plotted a profile comparing the distribution of the H content measured by ERDA and the one measured from FTIR for fluid inclusions

(Figure 3). The profiles in the fibrous habit are similar, the one from FTIR exhibiting lower values.

4. Discussion

4.1. Relationship between H content and H peaks height.

The absence of correlation between the values obtained by both methods, as highlighted by Figure 4, confirms what was hypothesized by the only other study[49] comparing ERDA and FTIR results. Not all H measured by ERDA comes from infrared active defects. Consequently, we classified each growth in four categories: A “low H” group (octahedral growth of CARTI1, PSC6 and VEN03); A “high H” group (cuboid sector of ASTER); An “intermediate H” group (octahedral sector of ASTER); A “high water” content group (fibrous sector of CARTI1).

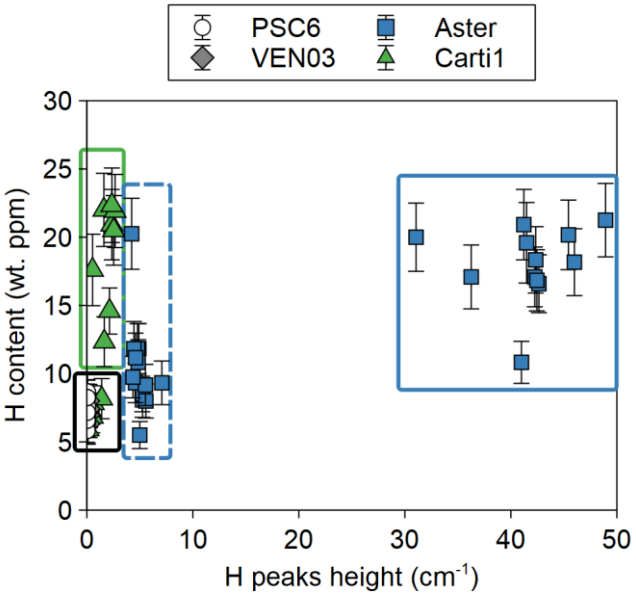

Figure 4. Comparison of the H peaks height measured by FTIR and the total hydrogen content measured by ERDA. The lack of correlation highlights that not all H in diamonds is IR active. Each growth habit can be classified in distinct categories based on H distribution (see text). For the asteriated diamond, the bold blue line is corresponding to the cuboid sector when the dashed blue lines is corresponding to the octahedral one. For the coated diamond, the dark bold line octahedral is corresponding to the octahedral core when the green bold line is corresponding to the fibrous rim.

4.2. H incorporation in monocrystalline octahedral and cuboid growths.

Since PSC6 is a commercial diamond window, we do not have any information on its preparation conditions. We do suspect that the original diamond was laser cut which could have removed some of, if not all, the H in the sample during the preparation. However, PSC6 shows the same range of H content values as VEN03 who was cryo-polished to preserve the H in the diamond and in the inclusion. This could mean that the sample preparation, whether it is laser cutting or ion beam milling, does not affect the H within the sample.

The octahedral sector of ASTER is different from the other octahedral growths since its H content and its summed H peaks height are higher. The same observation can be applied to its cuboid sector which shows a combination of the highest H content and summed H peaks height measured in any diamond of this study. The difference of H incorporation between the octahedral and cuboid sectors has already been observed in previous studies on asteriated diamonds [38,51,52]. Since most analyses were conducted using optical techniques such as

UV-Vis or FTIR spectroscopies, there was no information on whether this observation could also be applied to the total H content. Our results confirm that the cuboid sectors incorporate more H than the octahedral ones. More specifically, H seems to be far more incorporated as infrared active defects in the cuboid growth than the octahedral one. It has been hypothesized that kinetics could be the main driving force behind the different growth habits of diamonds, with the cuboid sector growing much faster than the octahedral one [53]. The reason behind the simultaneous growth of these two habits in asteriated diamonds is still unknown, although H might be playing an important role based on the difference of incorporation between the cuboid and octahedral habits.

4.3. H incorporation in fibrous growths.

The low H peaks height combined with the presence of water related absorption bands on the FTIR spectrum of the fibrous habit of CARTI1 hinted an additional contribution from the fluid inclusions to the H content (Figure 3). Fibrous diamonds are known to contain a high density of inclusions between their fibers. These inclusions, either fluid or solid, are usually composed of a mix of a hydrous saline, a silicic and a carbonatitic endmembers [54]. The fibrous habit is also believed to grow much faster than the monocrystalline cuboid habit, which often leads to the encapsulation of their growth medium (fluids or melts) as inclusions [55]. Studies on the micro-fluid inclusions in natural diamonds associate the simultaneous presence of the bands around 1600 cm^{-1} (H–O–H bending) and 3400 cm^{-1} (O–H stretching) to the presence of water molecules, indicating that the fibrous inclusions in the fibrous coat of CARTI1 are mostly water.

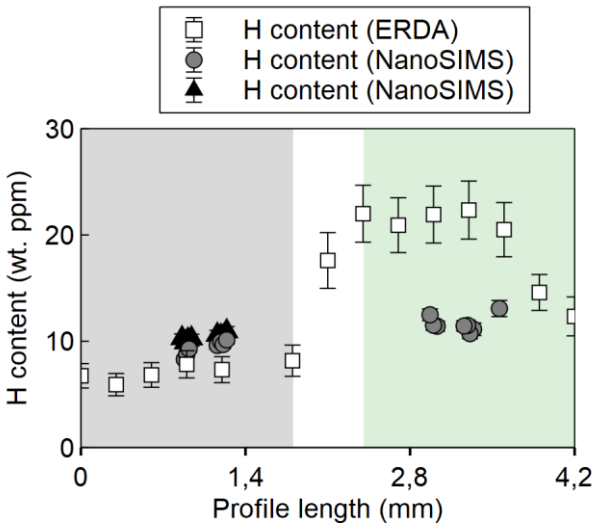

Figure 5. Profile of the total H content measured by ERDA (white squares) and NanoSIMS (grey circle, black triangles) in the octahedral (grey region) and the fibrous sectors (green region) of CARTI1. Grey circles represent analyses made on top of ERDA spots while black triangles represent analyses made next to ERDA spots.

In Figure 3C, we observed that H contents measured by ERDA is higher than measured by FTIR (related to fluid inclusions). This suggests that fibrous diamond matrix also contains H. This is confirmed when comparing the H contents measured by ERDA and NanoSIMS (Figure 5). Whereas the H contents in the octahedral sector are similar for both methods, those measured in the fibrous coat are smaller in NanoSIMS than in ERDA (Figure 5, Table 1). Since NanoSIMS probes about 120 nm, most of the fluid inclusions are eroded during the pre-sputtering step preceding the analysis. Hence, a major part of H from the fluid inclusions is lost before acquisition and the detected H can be attributed to the fibrous matrix itself. For this diamond, the H content of the fibrous sector seems to be a little higher than in the octahedral one.

Comparison between ERDA, FTIR and NanoSIMS suggests that the distribution of H within one sector is homogeneous at the micrometer scale.

4.4. Relationship between H and N.

Nitrogen, which defines type I diamonds, has already been thoroughly studied in the past [50]. From DFT calculation studies, it is proposed that H is mainly located in the N_3VH defect [24]. This would suggest a strong relationship between N and H incorporation in diamond. However, no correlation is observed between H and N contents of the series of diamonds analyzed in the present study (Fig. 6). Even for octahedral diamonds PSC6, VEN03 and the core of the coated diamond CARTI, where the H contents are similar, the N contents significantly differ. We observed less nitrogen in the cuboid sector of ASTER than in the octahedral one.

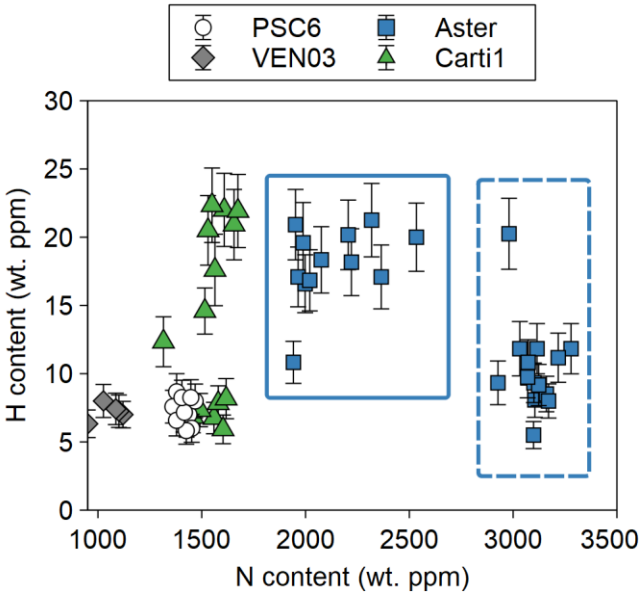

Figure 6. Comparison of the total N content measured by FTIR and the total H content measured by ERDA. The lack of correlation highlights/hints that there is not any relation between H and N. Two domains are observed in the asteriated diamond corresponding to octahedral (bold blue line) and cuboid (dashed blue line) sectors.

4.5. H incorporation in natural diamonds and implication for its cycle in the deep Earth.

Other than H, natural diamonds incorporate nitrogen and boron as major elemental impurities. With a content that can reach up to a few thousand wt. ppm, nitrogen is considered as the main impurity in natural diamonds. Boron on the other hand, which defines type IIb diamonds is shown to reach up to 10 wt. ppm [5]. With a range of measured values between 5 and 25 wt. ppm, H places itself as the second most abundant impurity in natural diamonds. These values are much lower than the observed few hundreds wt. ppm estimated by Nuclear Reaction Analysis [20]. Taking into account these values would mean that the amount of H incorporated into natural diamonds might vary in a larger range, but still below the range observed for N.

Another notable feature is the H content of asteriated diamonds, highest in the cuboid sector than the octahedral one, as also observed for N [38] which would imply that the incorporation of N and H is not dependent of the common parent fluid composition for the two simultaneously grown sectors.

H being the smallest element of the periodic table is assumed to diffuse fast in every material it is incorporated into, natural diamonds included. If H did diffuse as fast as claimed [56], then

ASTER would not have kept this notable difference between its two growth sectors during a long time of residence deep in the mantle. Instead, H would have been re-equilibrated in the diamond. The significant difference between the growth sectors of ASTER indicates the opposite. This lack of re-equilibration could be explained by H being inserted in energetically favorable centers, like a covalent C–H bond. We propose that the H distribution in natural diamonds has been preserved since their formation.

Studying the H content of diamond inclusions is crucial since, compared to mantle xenoliths whose H content was modified during their ascent to the surface [28], they are preserved by their host. These inclusions can be analyzed by FTIR [57,58]. With ERDA, it is possible to simultaneously determine the H content of the inclusion and the diamond which allows, in the case of syngenetic inclusions, the determination of a partition coefficient. Hydrogen incorporation in natural diamonds may be dependent on several factors during the growth (composition of the parent fluids or melts, growth rate, depth and environment of growth such as redox conditions). Diamonds form in fluids or melts which can be water-rich as seen in the fibrous habit of CARTI1 [47] and as also shown in many experimental studies [59], and thus can be considered as a reliable way to study the cycle of H in the deep Earth. All these factors should be considered to better understand how hydrogen incorporates itself in natural diamond and, thus, in the mantle.

5. Conclusion.

Through the combination of ERDA, FTIR and NanoSIMS, we acquired a better understanding of how H incorporates into diamonds. While ERDA is sufficient on its own and gives us the total H content in diamonds, FTIR cannot be used for quantification since not all H is infrared active. Each method has however its advantages: with ERDA, it is possible to quantify H in the diamond and its inclusions (fluid or mineral) at the same time. NanoSIMS measurements gives access to the H content at the microscale of the fibrous diamonds with little to no contamination from the fluid inclusions, which nature and content can be determined with FTIR, and witnesses for the homogeneous repartition of H within a same sector.

The current range of measured H content in natural diamonds varies from 5 to 25 wt. ppm, making it the second most abundant impurity incorporated in their structure after nitrogen and before boron. There seem to be no relationships between the incorporation of H and N in the diamond lattice. The quantity of H and its main mode of incorporation change with the diamond growth habit. Within the analyzed samples, the cuboid growth contained the highest amount of H, followed by the fibrous and the octahedral growths. H is mostly incorporated as infrared inactive defects in octahedral habits while it is mostly found in active defects in the cuboid ones. In case of the fibrous habit, a part of the H was incorporated in H containing defects while the other came from aqueous fluids inclusions embedded between the diamond fibers. Since there is not much known about the proportion of the infrared inactive defects, FTIR cannot be used for H absolute quantification.

Natural diamonds can be used to probe the cycle of H in the deep Earth. Our results suggest that H does not re-equilibrate in the lattice during its time of residence in the mantle, as seen by the significant difference of distribution between the two growth sectors of the asteriated diamond. Fluid inclusions in fibrous diamonds give a direct insight on the composition of their growth medium, which can be rich in water. Since natural diamonds are the only preserved geological samples that come from the deepest parts of the planet interior, measuring their total H content (diamond and inclusions) will help us better constrain its distribution in the deep Earth.

Acknowledgment

The project was funded by the IdEx Emergences 2019 Hydrodiams program (Sorbonne Universit´e). Cryo-ion polishing was performed at the FIB and SEM facility of IMPMC which is supported by Région Ile de France Grant SESAME 2006 NOI-07-593/R, Institut National des Sciences de l'Univers (INSU)–CNRS, Institut de physique–CNRS, Sorbonne Université, and the French National Research Agency (ANR) grant ANR-07-BLAN-0124-01. The NanoSIMS facility at the Muséum National d'Histoire Naturelle in Paris was established by funds from the CNRS, Région Ile de France, Ministère délégué à l'Enseignement supérieur et à la Recherche, and the Muséum National d'Histoire Naturelle. We thank Yvan-Pierre Kilisky for accelerator operation, Maxime Guillaumet for his assistance during FTIR measurements and also Stefan Kubsky and Mathieu Chevrot for AFM measurements on Diamonds. Two anonymous reviewers and the Editor Ken Haenen are thanked for their comments.

References

[1] B. Harte, Diamond formation in the deep mantle: the record of mineral inclusions and their distribution in relation to mantle dehydration zones, Mineral. Mag. 74 (2010) 189–215. https://doi.org/10.1180/minmag.2010.074.2.189.

[2] S.B. Shirey, P. Cartigny, D.J. Frost, S. Keshav, F. Nestola, P. Nimis, D.G. Pearson, N.V. Sobolev, M.J. Walter, Diamonds and the Geology of Mantle Carbon, Rev. Mineral. Geochem. 75 (2013) 355–421. https://doi.org/10.2138/rmg.2013.75.12.

[3] P. Cartigny, Stable Isotopes and the Origin of Diamond, Elements. 1 (2005) 79–84. https://doi.org/10.2113/gselements.1.2.79.

[4] P. Cartigny, M. Palot, E. Thomassot, J.W. Harris, Diamond Formation: A Stable Isotope Perspective, Annu. Rev. Earth Planet. Sci. 42 (2014) 699–732. https://doi.org/10.1146/annurev-earth-042711-105259.

[5] E. Gaillou, J.E. Post, D. Rost, J.E. Butler, Boron in natural type IIb blue diamonds: Chemical and spectroscopic measurements, Am. Mineral. 97 (2012) 1–18. https://doi.org/10.2138/am.2012.3925.

[6] Q. Williams, R.J. Hemley, Hydrogen in the Deep Earth, Annu. Rev. Earth Planet. Sci. 29 (2001) 365–418. https://doi.org/10.1146/annurev.earth.29.1.365.

[7] S. Demouchy, N. Bolfan-Casanova, Distribution and transport of hydrogen in the lithospheric mantle: A review, Lithos. 240–243 (2016) 402–425. https://doi.org/10.1016/j.lithos.2015.11.012.

[8] I.H. Campbell, S.R. Taylor, No water, no granites - No oceans, no continents, Geophys. Res. Lett. 10 (1983) 1061–1064. https://doi.org/10.1029/GL010i011p01061.

[9] G. Hirth, D.L. Kohlstedt, Water in the oceanic upper mantle: implications for rheology, melt extraction and the evolution of the lithosphere, Earth Planet. Sci. Lett. 144 (1996) 93–108. https://doi.org/10.1016/0012-821X(96)00154-9.

[10] K. Mierdel, H. Keppler, J.R. Smyth, F. Langenhorst, Water Solubility in Aluminous Orthopyroxene and the Origin of Earth's Asthenosphere, Science. 315 (2007) 364–368. https://doi.org/10.1126/science.1135422.

[11] E. Ohtani, Water in the Mantle, Elements. 1 (2005) 25–30. https://doi.org/10.2113/gselements.1.1.25.

[12] N. Bolfan-Casanova, Water in the Earth's mantle, Mineral. Mag. 69 (2005) 229–257. https://doi.org/10.1180/0026461056930248.

[13] C.H. van der Bogert, C.P. Smith, T. Hainschwang, S.F. McClure, Gray-to-Blue-to-Violet Hydrogen-Rich Diamonds from The Argyle Mine, Australia, Gems Gemol. 45 (2009) 20–37. https://doi.org/10.5741/GEMS.45.1.20.

[14] A. Tallaire, J. Achard, F. Silva, O. Brinza, A. Gicquel, Growth of large size diamond single crystals by plasma assisted chemical vapour deposition: Recent achievements and remaining challenges, Comptes Rendus Phys. 14 (2013) 169–184. https://doi.org/10.1016/j.crhy.2012.10.008.

[15] I.Z. Machi, S.H. Connell, P. Schaaff, B.P. Doyle, R.D. Maclear, K. Bharuth-Ram, P. Formenti, J.P.F. Sellschop, Hydrogen mobility in diamond studies using HI-ERDA

microscopy, Nucl. Instrum. Methods Phys. Res. Sect. B Beam Interact. Mater. At. 127–128 (1997) 212–216. https://doi.org/10.1016/S0168-583X(97)00067-0.
[16] B.P. Doyle, R.D. Maclear, S.H. Connell, P. Formenti, I.Z. Machi, J.E. Butler, P. Schaaff, J.P.F. Sellschop, E. Sideras-Haddad, K. Bharuth-Ram, 3-D-micro-ERDA microscopy of trace hydrogen distributions in diamond using a 2-D-PSD with event reconstruction, Nucl. Instrum. Methods Phys. Res. Sect. B Beam Interact. Mater. At. 130 (1997) 204–210. https://doi.org/10.1016/S0168-583X(97)00367-4.
[17] R.D. Maclear, S.H. Connell, B.P. Doyle, I.Z. Machi, J.E. Butler, J.P.F. Sellschop, S.R. Naidoo, E. Fritsch, Quantitative trace hydrogen distributions in natural diamond using 3D-micro-ERDA microscopy, Nucl. Instrum. Methods Phys. Res. Sect. B Beam Interact. Mater. At. 136–138 (1998) 579–582. https://doi.org/10.1016/S0168-583X(97)00701-5.
[18] R.J. Sweeney, V.M. Prozesky, K.S. Viljoen, S. Connell, The sensitive determination of H in diamond by infrared (FTIR) spectroscopy and micro-elastic-recoil (μ-ERDA) techniques, Nucl. Instrum. Methods Phys. Res. Sect. B Beam Interact. Mater. At. 158 (1999) 582–587. https://doi.org/10.1016/S0168-583X(99)00367-5.
[19] E. Sideras-Haddad, S.H. Connell, J.P.F. Sellschop, I.Z. Machi, D. Rebuli, R.D. Maclear, B.P. Doyle, Hydrogen and oxygen chemistry and dynamics in diamond studied by nuclear microscopic techniques, Nucl. Instrum. Methods Phys. Res. Sect. B Beam Interact. Mater. At. 181 (2001) 419–425. https://doi.org/10.1016/S0168-583X(01)00595-X.
[20] J.P.F. Sellschop, Nuclear probes in the study of diamond, in: Prop. Nat. Synth. Diam., Academic Press, 1992: pp. 81–180.
[21] A.M. Zaitsev, Optical Properties of Diamond, Springer, Berlin, Heidelberg, 2001. https://doi.org/10.1007/978-3-662-04548-0.
[22] E. Fritsch, T. Hainschwang, L. Massi, B. Rondeau, Hydrogen-Related Optical Centers in Natural Diamond: An Update, New Diam. Front. Carbon Technol. 17 (2007) 27.
[23] G.S. Woods, A.T. Collins, Infrared absorption spectra of hydrogen complexes in type I diamonds, J. Phys. Chem. Solids. 44 (1983) 471–475. https://doi.org/10.1016/0022-3697(83)90078-1.
[24] J.P. Goss, P.R. Briddon, V. Hill, R. Jones, M.J. Rayson, Identification of the structure of the 3107 cm^{-1} H-related defect in diamond, J. Phys. Condens. Matter. 26 (2014) 145801. https://doi.org/10.1088/0953-8984/26/14/145801.
[25] E. Fritsch, K. Scarratt, Gemmological properties of Type Ia diamonds with an unusually high hydrogen content, J. Gemmol. 23 (1993) 451–460. https://doi.org/10.15506/JoG.1993.23.8.451.
[26] H. Bureau, C. Raepsaet, H. Khodja, A. Carraro, C. Aubaud, Determination of hydrogen content in geological samples using elastic recoil detection analysis (ERDA), Geochim. Cosmochim. Acta. 73 (2009) 3311–3322. https://doi.org/10.1016/j.gca.2009.03.009.
[27] C. Raepsaet, H. Bureau, H. Khodja, C. Aubaud, A. Carraro, μ-Erda developments in order to improve the water content determination in hydrous and nominally anhydrous mantle phases, Nucl. Instrum. Methods Phys. Res. Sect. B Beam Interact. Mater. At. 266 (2008) 1333–1337. https://doi.org/10.1016/j.nimb.2008.01.028.
[28] N. Bolfan-Casanova, F. Schiavi, D. Novella, H. Bureau, C. Raepsaet, H. Khodja, S. Demouchy, Examination of Water Quantification and Incorporation in Transition Zone Minerals: Wadsleyite, Ringwoodite and Phase D Using ERDA (Elastic Recoil Detection Analysis), Front. Earth Sci. 6 (2018) 75. https://doi.org/10.3389/feart.2018.00075.
[29] J.L. Mosenfelder, A. von der Handt, A.C. Withers, H. Bureau, C. Raepsaet, G.R. Rossman, Coupled hydrogen and fluorine incorporation in garnet: New constraints from FTIR, ERDA, SIMS, and EPMA, Am. Mineral. 107 (2022) 587–602. https://doi.org/10.2138/am-2021-7880.
[30] V. Malavergne, H. Bureau, C. Raepsaet, F. Gaillard, M. Poncet, S. Surblé, D. Sifré, S. Shcheka, C. Fourdrin, D. Deldicque, H. Khodja, Experimental constraints on the fate of H and C during planetary core-mantle differentiation. Implications for the Earth, Icarus. 321 (2019) 473–485. https://doi.org/10.1016/j.icarus.2018.11.027.

[31] C. Aubaud, H. Bureau, C. Raepsaet, H. Khodja, A.C. Withers, M.M. Hirschmann, D.R. Bell, Calibration of the infrared molar absorption coefficients for H in olivine, clinopyroxene and rhyolitic glass by elastic recoil detection analysis, Chem. Geol. 262 (2009) 78–86. https://doi.org/10.1016/j.chemgeo.2009.01.001.
[32] V. Clesi, M.A. Bouhifd, N. Bolfan-Casanova, G. Manthilake, F. Schiavi, C. Raepsaet, H. Bureau, H. Khodja, D. Andrault, Low hydrogen contents in the cores of terrestrial planets, Sci. Adv. 4 (2018) e1701876. https://doi.org/10.1126/sciadv.1701876.
[33] A.C. Withers, H. Bureau, C. Raepsaet, M.M. Hirschmann, Calibration of infrared spectroscopy by elastic recoil detection analysis of H in synthetic olivine, Chem. Geol. 334 (2012) 92–98. https://doi.org/10.1016/j.chemgeo.2012.10.002.
[34] D. Lévy, J. Aléon, A. Aléon-Toppani, D. Troadec, R. Duhamel, A. Gonzalez-Cano, H. Bureau, H. Khodja, NanoSIMS Imaging of D/H Ratios on FIB Sections, Anal. Chem. 91 (2019) 13763–13771. https://doi.org/10.1021/acs.analchem.9b03134.
[35] S. Azevedo-Vannson, L. Remusat, H. Bureau, K. Béneut, B. Cesare, H. Khodja, M. Jiménez-Mejías, M. Roskosz, Nanoscale Secondary Ion Mass Spectrometry determination of the water content of staurolite, Rapid Commun. Mass Spectrom. 36 (2022) e9331. https://doi.org/10.1002/rcm.9331.
[36] J. Aléon, D. Lévy, A. Aléon-Toppani, H. Bureau, H. Khodja, F. Brisset, Determination of the initial hydrogen isotopic composition of the solar system, Nat. Astron. (2022). https://doi.org/10.1038/s41550-021-01595-7.
[37] J.W. Harris, K.V. Smit, Y. Fedortchouk, M. Moore, Morphology of Monocrystalline Diamond and its Inclusions, Rev. Mineral. Geochem. 88 (2022) 119–166. https://doi.org/10.2138/rmg.2022.88.02.
[38] B. Rondeau, E. Fritsch, M. Guiraud, J.-P. Chalain, F. Notari, Three historical 'asteriated' hydrogen-rich diamonds: growth history and sector-dependent impurity incorporation, Diam. Relat. Mater. 13 (2004) 1658–1673. https://doi.org/10.1016/j.diamond.2004.02.002.
[39] L. Daver, H. Bureau, É. Boulard, É. Gaillou, P. Cartigny, D.L. Pinti, O. Belhadj, N. Guignot, E. Foy, I. Estève, B. Baptiste, From the lithosphere to the lower mantle: An aqueous-rich metal-bearing growth environment to form type IIb blue diamonds, Chem. Geol. 613 (2022) 121163. https://doi.org/10.1016/j.chemgeo.2022.121163.
[40] H. Khodja, E. Berthoumieux, L. Daudin, J.-P. Gallien, The Pierre Süe Laboratory nuclear microprobe as a multi-disciplinary analysis tool, Nucl. Instrum. Methods Phys. Res. Sect. B Beam Interact. Mater. At. 181 (2001) 83–86. https://doi.org/10.1016/S0168-583X(01)00564-X.
[41] P. Cartigny, F. Pineau, C. Aubaud, M. Javoy, Towards a consistent mantle carbon flux estimate: Insights from volatile systematics (H2O/Ce, δD, CO2/Nb) in the North Atlantic mantle (14° N and 34° N), Earth Planet. Sci. Lett. 265 (2008) 672–685. https://doi.org/10.1016/j.epsl.2007.11.011.
[42] W.-F. Zhang, X.-P. Xia, T. Eiichi, L. Li, Q. Yang, Y.-Q. Zhang, Y.-N. Yang, M.-L. Liu, C. Lai, Optimization of SIMS analytical parameters for water content measurement of olivine, Surf. Interface Anal. 52 (2020) 224–233. https://doi.org/10.1002/sia.6729.
[43] M. Mayer, SIMNRA, a simulation program for the analysis of NRA, RBS and ERDA, AIP Conf. Proc. 475 (1999) 541–544. https://doi.org/10.1063/1.59188.
[44] D. Howell, C.J. O'Neill, K.J. Grant, W.L. Griffin, N.J. Pearson, S.Y. O'Reilly, μ-FTIR mapping: Distribution of impurities in different types of diamond growth, Diam. Relat. Mater. 29 (2012) 29–36. https://doi.org/10.1016/j.diamond.2012.06.003.
[45] H. Bureau, L. Remusat, I. Esteve, D.L. Pinti, P. Cartigny, The growth of lithospheric diamonds, Sci. Adv. 4 (2018) eaat1602. https://doi.org/10.1126/sciadv.aat1602.
[46] A. Thomen, F. Robert, L. Remusat, Determination of the nitrogen abundance in organic materials by NanoSIMS quantitative imaging, J. Anal. At. Spectrom. 29 (2014) 512–519. https://doi.org/10.1039/C3JA50313E.
[47] O. Navon, I.D. Hutcheon, G.R. Rossman, G.J. Wasserburg, Mantle-derived fluids in diamond micro-inclusions, Nature. 335 (1988) 784–789. https://doi.org/10.1038/335784a0.

[48] D. Howell, Y. Weiss, K. Smit, L. Loudin, F. Nestola, DiaMap: New applications for processing IR spectra of fluid-rich diamonds and mapping diamonds containing isolated nitrogen (Type Ib) and boron (Type IIb), in: 2017. https://doi.org/10.1130/abs/2017AM-298964.
[49] R.J. Sweeney, V.M. Prozesky, K.S. Viljoen, S. Connell, The sensitive determination of H in diamond by infrared (FTIR) spectroscopy and micro-elastic-recoil (I-ERDA) techniques, (1999) 6.
[50] M.N.R. Ashfold, J.P. Goss, B.L. Green, P.W. May, M.E. Newton, C.V. Peaker, Nitrogen in Diamond, Chem. Rev. 120 (2020) 5745–5794. https://doi.org/10.1021/acs.chemrev.9b00518.
[51] D. Howell, W. Griffin, S. Piazolo, J. Say, R. Stern, T. Stachel, L. Nasdala, J. Rabeau, P. N.J, S. O'Reilly, A spectroscopic and carbon-isotope study of mixed-habit diamonds: Impurity characteristics and growth environment, Am. Mineral. 98 (2013) 66–77. https://doi.org/10.2138/am.2013.4179.
[52] K.V. Smit, S.B. Shirey, R.A. Stern, A. Steele, W. Wang, Diamond growth from C–H–N–O recycled fluids in the lithosphere: Evidence from CH 4 micro-inclusions and δ 13 C– δ 15 N–N content in Marange mixed-habit diamonds, Lithos. 265 (2016) 68–81. https://doi.org/10.1016/j.lithos.2016.03.015.
[53] I. Sunagawa, Growth and morphology of diamond crystals under stable and metastable contitions, J. Cryst. Growth. 99 (1990) 1156–1161. https://doi.org/10.1016/S0022-0248(08)80100-5.
[54] Y. Weiss, J. McNeill, D.G. Pearson, G.M. Nowell, C.J. Ottley, Highly saline fluids from a subducting slab as the source for fluid-rich diamonds, Nature. 524 (2015) 339–342. https://doi.org/10.1038/nature14857.
[55] R. Tappert, M.C. Tappert, Diamonds in nature: a guide to rough diamonds, Springer, Berlin Heidelberg, 2011.
[56] D.J. Cherniak, E.B. Watson, V. Meunier, N. Kharche, Diffusion of helium, hydrogen and deuterium in diamond: Experiment, theory and geochemical applications, Geochim. Cosmochim. Acta. 232 (2018) 206–224. https://doi.org/10.1016/j.gca.2018.04.029.
[57] D.G. Pearson, F.E. Brenker, F. Nestola, J. McNeill, L. Nasdala, M.T. Hutchison, S. Matveev, K. Mather, G. Silversmit, S. Schmitz, B. Vekemans, L. Vincze, Hydrous mantle transition zone indicated by ringwoodite included within diamond, Nature. 507 (2014) 221–224. https://doi.org/10.1038/nature13080.
[58] D. Novella, N. Bolfan-Casanova, F. Nestola, J.W. Harris, H2O in olivine and garnet inclusions still trapped in diamonds from the Siberian craton: Implications for the water content of cratonic lithosphere peridotites, Lithos. 230 (2015) 180–183. https://doi.org/10.1016/j.lithos.2015.05.013.
[59] R.W. Luth, Y.N. Palyanov, H. Bureau, Experimental Petrology Applied to Natural Diamond Growth, Rev. Mineral. Geochem. 88 (2022) 755–808. https://doi.org/10.2138/rmg.2022.88.14.